Available online at www.sciencedirect.com
ScienceDirect
Journal of Photochemistry and Photobiology A: Chemistry 186 (2007) 93–98
Journal of Photochemistry and Photobiology A:Chemistry
www.elsevier.com/locate/jphotochem

Photolysis of polycyclic aromatic hydrocarbons associated with fly ash particles under simulated sunlight irradiation

Junfeng Niu [a,*], Ping Sun [b], Karl-Werner Schramm [c]

[a] State Key Laboratory of Water Environment Simulation, School of Environment, Beijing Normal University, Beijing 100875, PR China
[b] School of Public and Environmental Affairs, Indiana University, Bloomington 47405, USA
[c] GSF-National Research Centre for Environment and Health, Institute of Ecological Chemistry, D-85764 Neuherberg, Germany

Received 14 April 2006; received in revised form 14 July 2006; accepted 27 July 2006
Available online 5 August 2006

Abstract

Fly ash particle-associated polycyclic aromatic hydrocarbons (PAHs) were produced by combustion of polyvinyl chloride (PVC), wood, high-density polyethylene (HDPE), and polystyrene in a stove. Fly ash particles were deposited on the glass slides (76 mm × 26 mm) placed in the exposure chamber. The concentration of 16 PAHs ranged from 10.1 pg/dm^2 fly ash for acenaphthene to 2348.7 pg/dm^2 fly ash for fluoranthene. Medium to large molecular weight PAH concentrations were much higher compared to low molecular weight PAHs on fly ash. Photolysis of PAHs associated with fly ash particles deposited on glass slides was investigated under simulated sunlight irradiation for about 550 h. Generally, the photolysis rates of the 16 PAHs follow first-order kinetics. Under simulated sunlight containing UV-B, the photolysis of PAHs includes two phases: fast (0–50 h) and slow phase (50–550 h). The photolysis rate constants of PAHs in the initial fast phase were far greater than those in the slow phase. When UV-B was removed from the simulated sunlight irradiation, the photolysis rate constants of PAHs were significantly lower compared to those observed in the fast phase with UV-B exposure, suggesting UV-B radiation could accelerate photolysis of PAHs adsorbed on the fly ash particles. In addition, partial least squares (PLS) analysis models were applied to explain the molecular structural characteristics that affect the PAH photolysis rates. The results suggested that the photolysis rate constants of PAHs decrease with the increasing of molecular weight (M_w), the energy of the lowest unoccupied molecular orbital (E_{LUMO}), $E_{LUMO} + E_{HOMO}$, and the standard heat of formation (ΔH_f).

Keywords: Photolysis; PAHs; Fly ash; Partial least squares; Simulated sunlight

1. Introduction

Polycyclic aromatic hydrocarbons (PAHs) are primarily produced by incomplete combustion of fossil fuels and natural material (e.g. forest and prairie fires, agricultural burning). Some PAHs are considered priority pollutants with great potential risk to human health [1,2]. Because of the high toxicity and potential adverse effects on human beings and the wildlife, PAHs have been extensively investigated, particularly their transport and transformation in the environment [3–5].

Photolysis is an important transformation pathway for most PAHs in the environment [6–9]. Photochemical reactions of PAHs can occur in surface water, atmosphere, or on the surface of soil [3,6,10]. For example, Zepp and Schlotzhauer [6] found that the photolysis rates of selected PAHs in natural water body were quite fast, the photolysis half-lives ($t_{1/2}$) of PAHs ranged from minutes to a few hours. This conclusion was later supported by other studies [8,9,11]. Fast photolytic reaction rates of PAHs in organic solvents have also been reported [12]. However, the photodegradation of PAHs on solid and atmospheric particulates was much slower than in water and organic solvent [13–16].

Under sunlight irradiation, photolysis may be one of the major abiotic transformations of these chemicals adsorbed on the particles in the atmosphere. It has been suggested that photochemical fate of PAHs was dependent on the substrate on which they are adsorbed [13–15]. The more common assumption is that the airborne particulate matter and fly ash from combustion can stabilize the photolysis of PAHs and facilitate their transport from combustion sources in the atmosphere [13–16]. These previous studies were generally conducted for short time (e.g.

* Corresponding author. Tel.: +86 10 5880 5053; fax: +86 10 5880 2018.
E-mail address: junfengn@bnu.edu.cn (J. Niu).

1010-6030/$ – see front matter © 2006 Elsevier B.V. All rights reserved.
doi:10.1016/j.jphotochem.2006.07.016

less than 100 h). So far, the photochemical behavior of PAHs associated with fly ash particles for a longer period is still not well understood.

The aim of this study is to investigate the photochemical behavior of PAHs associated with fly ash particles under long-term simulated sunlight irradiation. In addition, partial least squares (PLS) analysis models were developed to explain the molecular structural characteristics that could affect the PAH photolysis rates.

2. Materials and methods

2.1. Generation of PAHs

The fly ash samples were prepared from a combustion system that has been described in detail in a previous study [17]. In brief, a mixture of polyvinyl chloride (PVC), wood, high-density polyethylene (HDPE), and polystyrene was used for combustion to produce exhaust gas containing fly ash particle-associated PAHs. Fly ash particles were deposited on the glass slides (76 mm × 26 mm) placed in the exposure chamber, where the temperature was held at about 32 °C. The glass slides were kept in the exposure chamber for 96 h after combustion. Some big fly ash particles were blown off from the glass slide surface using gentle N_2 flow to establish a uniform and consistent distribution of PAH concentration.

2.2. Simulated sunlight exposure

PAHs associated with fly ash particles were exposed to simulated sunlight to study their photolytic behavior. The simulated sunlight was used because it is controllable, reproducible, and reasonably representative of natural sunlight. The experiments were conducted in two sunlight simulators, chambers A and B. The irradiance spectrums of the simulated sunlight in chambers A and B are shown in Fig. 1. The dimension of the controlled environmental chambers and experimental conditions were described elsewhere [18]. In both chambers, the light and UV-radiation were set at moderate levels normally occurring at mid-latitudes. In chamber A, the integrated irradiance at canopy level was 840–940 μmol m^{-2} s^{-1} for photosynthetic active radiation (PAR) (400–700 nm), which corresponds to a total global irradiance in the order of 400 W m^{-2} and 11–16 W m^{-2} for UV-A (315–400 nm), and 0.43–0.53 W m^{-2} for UV-B (280–315 nm). The range of irradiance values considers the spatial distribution of light and UV-radiation within the chamber. In chamber B, the UV-B component was almost completely removed (<10^{-4} W m^{-2}) using appropriate glass filters while the other light and radiation parameters were the same as in chamber A.

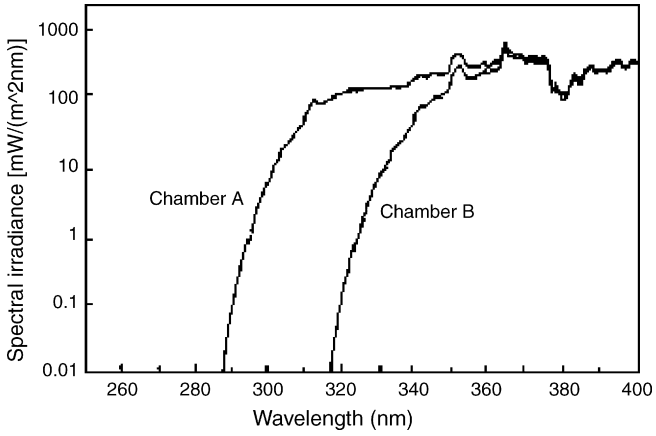

Fig. 1. The spectral irradiance of simulated sunlight in chambers A and B.

2.3. Analytical methods

Ten glass slides fully exposed to simulated sunlight in both chamber A and chamber B were periodically sampled throughout the experiment for PAH analysis. These glass slides were rinsed with hexane/acetone (2:1, v/v) for three times and extracted in a 100 ml centrifuge tube for 1.0 h using an ultrasonic bath (RK-156, Bandelin, Berlin, Germany). Five microgram of ^{2}H-labeled PAHs (Cambridge Isotope Laboratory, Woburn, MA, USA) was added into each sample prior to extraction to monitor extraction efficiency. The samples were then shaken for 1.0 h at 500 rpm by a constant temperature shaker to ensure the thoroughly intermixing. The extracts was eluted with 8 ml hexane using a column filled with 2.0 g silica gel (5% deactivated) in lower part and 1.0 g Na_2SO_4 in upper part, followed with 8 ml hexane/dichloromethane (1:1, v/v). The fraction containing the PAHs was concentrated to 1 ml by a rotary evaporator and added 1 μg of pentachlorotoluene prior to gas chromatograph–mass spectrometry (GC/MS) analysis.

Quantification of PAHs was performed on a GC/MS system (Fisons GC 8060, MS: MD800) with a DB-XLB capillary column (30 m × 0.25 mm, 0.25 μm film thickness). Helium was used as carrier gas with a flow rate of 1.0 ml/min. One microlitre of samples was injected in the splitless mode. The MS was operated in the selected ion monitoring (SIM) mode. Sixteen PAHs were quantified in this study (see Table 1). Naphthalene was not included due to its high volatility and thus cannot be retained on the surfaces of fly ash particles.

2.4. Quantum chemical descriptors calculation

Some fundamental quantum chemical descriptors computed by PM3 Hamiltonian were obtained in order to explain the photolysis of PAHs sorbed on fly ash from the molecular structural characteristics. A total of 13 descriptors reflecting the overall characteristics of the PAHs were used in this study. The full list is given in Table 2. In addition, three combinations of frontier molecular orbital energies, $E_{LUMO} - E_{HOMO}$, $(E_{LUMO} - E_{HOMO})^2$ and $E_{LUMO} + E_{HOMO}$, were also selected as predictor variables because many applications are available on the use of these parameters as quantum descriptors to develop quantitative structure–property relationship (QSPR) models [19,20]. The $E_{LUMO} - E_{HOMO}$ and $E_{LUMO} + E_{HOMO}$ can be related to absolute hardness and electronegativity, respectively [21,22].

Table 1
The initial concentration and rate constants for the photolysis of PAHs on fly ash particles

PAH	C_0 (pg/dm^2)	Chamber A (PAR + UV-A + UV-B)		Chamber B (PAR + UV-A), k_B ($\times 10^3$ h^{-1}) (0–550 h)
		k_{A1} ($\times 10^3$ h^{-1}) (0–50 h)	k_{A2} ($\times 10^3$ h^{-1}) (50–550 h)	
Acenaphthylene	80 ± 3.6	9.1 ± 0.8	3.3 ± 0.3	4.6 ± 0.4
Acenaphthene	10 ± 1.5	7.8 ± 0.6	2.8 ± 0.4	4.3 ± 0.4
Fluorene	37 ± 3.1	7.7 ± 0.6	2.6 ± 0.3	3.7 ± 0.5
Phenanthrene	1200 ± 95	6.2 ± 0.4	2.6 ± 0.2	2.8 ± 0.2
Anthracene	140 ± 10	8.6 ± 0.7	3.7 ± 0.3	4.2 ± 0.4
Fluoranthene	2300 ± 140	4.5 ± 0.5	2.9 ± 0.2	3.3 ± 0.3
Pyrene	1500 ± 100	7.3 ± 0.4	2.4 ± 0.2	3.0 ± 0.3
Benzo[*a*]anthracene	1200 ± 78	5.0 ± 0.4	2.9 ± 0.3	3.4 ± 0.5
Cyclopenta[*c*,*d*]pyrene	1300 ± 100	3.2 ± 0.2	1.5 ± 0.3	2.1 ± 0.3
Benzo[*b*]fluoranthene	1800 ± 41	3.5 ± 0.2	1.2 ± 0.1	1.5 ± 0.2
Benzo[*k*]fluoranthene	400 ± 38	2.8 ± 0.1	1.4 ± 0.3	1.8 ± 0.4
Benzo[*e*]pyrene	620 ± 46	2.5 ± 0.1	1.4 ± 0.2	1.8 ± 0.3
Benzo[*a*]pyrene	420 ± 29	3.9 ± 0.2	2.3 ± 0.2	2.6 ± 0.4
Indeno[1,2,3-*cd*]pyrene	510 ± 29	3.8 ± 0.2	1.2 ± 0.1	1.5 ± 0.2
Dibenzo[*a*,*h*]anthracene	180 ± 7.5	3.5 ± 0.2	1.7 ± 0.3	2.1 ± 0.5
Benzo[*g*,*h*,*i*]perylene	430 ± 15	4.1 ± 0.2	2.3 ± 0.3	1.8 ± 0.4

Values represent mean ± S.D.

2.5. Statistical analysis

PLS algorithm, which is not only searching the relationship between a matrix **Y** (containing dependent variables) and a matrix **X** (containing predictor variables), but also reducing the dimension of the matrices while concurrently maximizing the relationship between the descriptors, was applied to analyze PAH photolysis affected by different molecular structure characteristics. Simca (Simca-S Version 6.0, Umetri AB and Erisoft AB) software was used to perform PLS analysis. The conditions for the computation were based on the default values of the software. The criteria used to determine the model dimensionality (i.e. the number of significant PLS components) is cross validation (CV). With CV, the fraction of the total variation of the dependent variables can be predicted by a component, Q^2. The tested PLS component is considered significant if the whole data set has a Q^2-value larger than a significance limit (0.097).

Table 2
Molecular structural descriptors of PAHs

Symbols	Description
M_w	Molecular weight
ΔH_f	Standard heat of formation (kcal mol^{-1})
TE	Total energy (eV)
EE	Electronic energy (eV)
CCR	Core–core repulsion energy (eV)
E_{HOMO}	The energy of the highest occupied molecular orbital (eV)
E_{HOMO-1}	The energy of the second highest occupied molecular orbital (eV)
E_{LUMO}	The energy of the lowest unoccupied molecular orbital (eV)
E_{LUMO+1}	The energy of the second lowest unoccupied molecular orbital (eV)
Q_H^+	The most positive net atomic charges on a hydrogen atom (a.c.u.)
Q_C^-	The largest negative atomic charge on a carbon atom (a.c.u.)
μ	Dipole moment (a.u.)
α	Average molecular polarizability (a.u.)

When the cumulative Q^2 for the extracted components, Q^2_{cum}, is larger than 0.5, the model is considered to have a good prediction ability. Model adequacy was mainly measured as the number of PLS principal components (A), Q^2_{cum}, the correlation coefficient between observed values and fitted values (R), the significance level (p), and the standard error (S.E.). S.E. was defined as:

$$\text{S.E.} = \sqrt{\frac{\sum_{i=1}^{n}[\log k(\text{observed})_i - \log k(\text{predicted})_i]^2}{n - A - 1}} \quad (1)$$

where n is the number of observations used for model building, and k stands for the photolysis rate constants of PAHs associated with fly ash particles under simulated sunlight irradiation.

3. Results and discussion

3.1. PAH concentration on fly ash particles

Generally, the total amount of fly ash collected from 10 glass slide surface was about 0.008 g. Due to this low mass content of fly ash, high error may occur if the mass of fly ash is involved to express concentration of PAHs on fly ash particles. We observed that the fly ash on the glass slides had very thin thickness and can be considered as consistent. Thus, the mass of PAHs per square decimeter of slide surface (pg/dm^2 fly ash) was used as the concentration unit to calculate photolysis kinetics.

Table 1 shows the initial concentration (C_0, pg/dm^2 fly ash) of each PAH sorbed on fly ash, which ranged from 10 ± 1.5 pg/dm^2 fly ash for acenaphthene to 2300 ± 140 pg/dm^2 fly ash for fluoranthene. Clearly, medium molecular weight PAHs were major components presented on fly ash particles. Fluoranthene, benzo[*b*]fluoranthene, pyrene, and cyclopenta[*c*,*d*]pyrene contributed more than 50% to the sum of 16 PAH concentration. In contrast, the concentrations of small molecular weight PAHs including fluorene, acenaphthene, and acenaphthylene were less than 1% of the total 16 PAH concentration, indicating that these

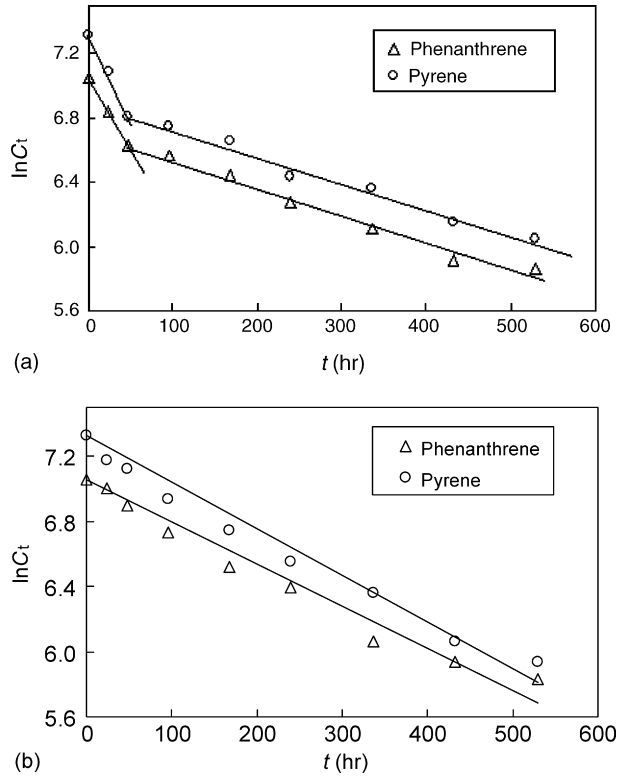

Fig. 2. The correlation between phenanthrene and pyrene concentrations on fly ash particles and irradiation time in chambers A (a) and B (b).

small molecular weight PAHs were almost negligible on fly ash particles. The PAH homolog pattern observed in our study is similar as those reported on fly ash generated from wood or plastic burning [23,24] except that the amount of phenanthrene in our study was slightly lower. As stated in Section 2, the big fly ash particles deposited on the glass slide surface were gently blown off by N_2 flow, which could lead to the lower phenanthrene concentration.

3.2. Photolysis kinetics of PAHs

For the experiments conducted in chamber A with simulated sunlight containing UV-B, the reaction kinetics of PAHs could be divided into two phases, as shown in Fig. 2a for phenanthrene and pyrene. The photolysis rates were considerably fast in the first phase (experimental time from 0 to 50 h), and then declined in the second phase (from 50 to 550 h). The correlations of the natural logarithms of PAH concentration ($\ln C_t$) versus time (t) are essentially straight lines for the two phases (Fig. 2a). Due to the low concentrations of PAHs in the fly ash samples, it is reasonable to assume the first-order kinetics. Thus, the first-order kinetics was applied to explain the photolysis of all the 16 PAHs on fly ash surfaces in chamber A. Interestingly, there was no distinction between the two phases for the experiments performed in chamber B (Fig. 2b). Instead, a simple linear correlation between $\ln C_t$ and exposure time t was observed for experiments conducted in chamber B. The photolysis rate constants of PAHs in chamber B were also calculated assuming that the photolysis follows the first-order kinetics.

The photolysis rate constants of all the 16 PAHs associated with fly ash particles exposed to simulated sunlight were shown in Table 1. In general, the rate constants in chamber B were much lower than those measured in the first phase in chamber A, but similar as the photolysis rate constants determined in the second phase in chamber A. For example, in the first phase of PAH photolysis in chamber A, the rate constant of phenanthrene was $(6.2 \pm 0.4) \times 10^{-3}\,h^{-1}$, which was significantly higher than $(2.6 \pm 0.2) \times 10^{-3}\,h^{-1}$ in the second phase. While in chamber B, the photolysis rate constant of phenanthrene was about $(2.8 \pm 0.2) \times 10^{-3}\,h^{-1}$, statistically similar as the value measured in second phase photolysis in chamber A. Because PAHs absorb both UV-A and UV-B radiation [25,26], both UV-A and UV-B may contribute to the direct photolysis of PAHs. In the present study, when UV-B was removed from the simulated sunlight irradiation, the photolysis rate constants of PAHs were significant lower compared to those observed in the fast phase with UV-B exposure, suggesting UV-B radiation could accelerate photolysis of PAHs adsorbed on the fly ash particles.

We also observed a generally decreasing trend of PAH photolysis rate constants with the increasing molecular weight. The maximum photolysis rate constant (for acenaphthylene) is approximately four times faster than the minimum value (for benzo[*e*]pyrene). Interestingly, PAHs with molecular weight larger than benzo[*a*]anthracene had much lower rate constants compared to low molecular weight PAHs. Behymer and Hites [15] studied photolysis of PAHs adsorbed on fly ash particles using a rotary photo-reactor, their results suggested a similar half-lives for all the PAHs. The difference between our study and Behymer and Hites [15] could presumably due to the longer experimental time (about 550 h) in our experiments compared to 25 h experimental time used by Behymer and Hites [15].

Photon absorption by the PAH molecules is a prerequisite for photochemical reaction. The higher photolysis rate constants of PAHs sorbed on fly ash in the initial phase (about 0–50 h) could be due to the more sorption of photons in this phase. In our experiments, only the fly ash surfaces were exposed to the simulated sunlight. Since fly ash may strongly attenuate light below their surfaces, PAHs embed in the interior of fly ash can hardly expose to the simulated sunlight resulting in lower photolysis rate in the second phase. In addition, in the second phase of photolysis kinetics in chamber A, the migration of particle-associated PAHs from the interior to exterior of fly ash could be the rate-limiting step and thus prohibit the photolysis of PAHs.

3.3. PLS analysis models

Variable importance in the projection (VIP) is a parameter in PLS analysis that shows the importance of a variable in a PLS model. Terms with a large value of VIP (e.g. larger than 1) are the most relevant for explaining dependent variable. PLS analysis with the PAH photolysis rate constants (Table 1) as dependent variables and the 16 quantum chemical descriptors as independent variables generated many results. The optimal model, which has the largest Q^2_{cum}, was obtained through stepwise culling the model with the smallest VIP value out. Following the analyt-

ical methods described above, models (1)–(3) were obtained for $\log k_{A1}$ (photolysis rate constant in phase 1 in chamber A), $\log k_{A2}$ (photolysis rate constant in phase 2 in chamber A), and $\log k_B$ (photolysis rate constant in chamber B), respectively:

- Model (1):

$$\log k_{A1} = -1.902 - 1.556 \times 10^{-3} M_w + 8.077 \times 10^{-5} TE + 7.063 \times 10^{-6} EE - 1.524 \times 10^{-2} \Delta H_f - 3.569 \times 10^{-2}(E_{LUMO} + E_{HOMO}),$$
$$n = 16, \quad A = 2, \quad Q^2_{cum} = 0.775, \quad R = 0.908,$$
$$p = 1.212 \times 10^{-6}, \quad S.E. = 0.082 \qquad (2)$$

- Model (2):

$$\log k_{A2} = -1.959 - 1.760 \times 10^{-3} M_w + 8.983 \times 10^{-5} TE - 1.341 \times 10^{-3} \Delta H_f - 6.963 \times 10^{-1} \mu - 3.531 \times 10^{-2} E_{LUMO},$$
$$n = 16, \quad A = 2, \quad Q^2_{cum} = 0.727, \quad R = 0.894,$$
$$p = 3.125 \times 10^{-6}, \quad S.E. = 0.077 \qquad (3)$$

- Model (3):

$$\log k_B = -1.950 - 1.150 \times 10^{-3} M_w + 6.386 \times 10^{-5} TE + 5.900 \times 10^{-6} EE - 9.777 \times 10^{-4} \Delta H_f - 6.493 \times 10^{-1} CCR - 1.777 \times 10^{-2} E_{LUMO},$$
$$n = 16, \quad Q^2_{cum} = 0.783, \quad R = 0.899,$$
$$p = 2.241 \times 10^{-6}, \quad S.E. = 0.078 \qquad (4)$$

As shown by models (1)–(3), all the correlations between the observed and predicted dependent values are significant. Moreover, as the cross-validated Q^2_{cum} values of models (1)–(3) are remarkably above 0.50, indicating that the three models are surely stable and have good prediction abilities. These model-fitting results are listed in Table 3.

The results obtained from the three models suggested that molecular structural characteristics of PAHs affect photochemical degradation of these molecules on fly ash particles. First, the photolysis rate constants of PAHs in chambers A and B decrease with the increasing of M_w and ΔH_f values, which agreed with our experimental observations on the lower photolysis rate constants of larger molecular weight PAHs. Increasing of TE values lead to the increasing of disappearance rates of PAHs. Second, model (1) indicates that the first PLS component is mainly related to the descriptors M_w, TE, EE and ΔH_f, for which the $W^*[1]$ value is larger than 0.440 and the absolute values of $W^*[1]$ for the other descriptors are given in Table 3. This implies that these descriptors are highly inter-correlated. TE and EE correlates with M_w negatively, as shown in Table 4. Thus, this approved again that the increasing of M_w values could lead to the decreasing of the $\log k_{A1}$ values of PAHs. The second PLS component is loaded primarily on the descriptor of $E_{LUMO} + E_{HOMO}$. As indicated by the pseudo-regression coefficient for $E_{LUMO} + E_{HOMO}$, PAH congeners with high $E_{LUMO} + E_{HOMO}$ values tend to be stable and difficult to be photolyzed on fly ash particles. According to Pearson [21], absolute electronegativity can be defined as $(E_{LUMO} + E_{HOMO})/2$. Therefore PAH molecules with bigger absolute electronegativity values tend to have higher $\log k_{A1}$ values and lead to faster photodegradation rates. Third, the first PLS component in model (2) is mainly related to the descriptors M_w,

Table 3
The variable importance in the projection (VIP) and PLS weights ($W^*[1]$ and $W^*[2]$) for the molecular structural descriptors included in models (1)–(3)

Variables	VIP	$W^*[1]$	$W^*[2]$
Model (1)			
M_w	1.185	−0.547	−0.370
TE	1.083	0.504	−0.086
EE	1.056	0.489	−0.142
ΔH_f	0.973	−0.448	−0.327
$E_{HOMO} + E_{LUMO}$	0.604	0.085	−0.869
Model (2)			
M_w	1.300	−0.640	−0.341
TE	1.099	0.535	−0.028
ΔH_f	1.033	−0.510	−0.088
μ	0.724	−0.191	−0.701
E_{LUMO}	0.715	0.081	−0.699
Model (3)			
M_w	1.114	−0.457	−0.458
TE	1.093	0.458	−0.001
EE	1.082	0.453	−0.034
CCR	1.080	−0.452	0.038
ΔH_f	0.859	−0.351	−0.300
E_{LUMO}	0.710	0.219	−0.841

Table 4
Correlation coefficients between some quantum chemical descriptors in models (1)–(3)

	M_w	ΔH_f	TE	EE	E_{LUMO}	CCR	$E_{LUMO} + E_{HOMO}$	μ
M_w	1.000							
ΔH_f	0.584	1.000						
TE	−0.894*	−0.589	1.000					
EE	−0.863*	−0.572	0.997*	1.000				
E_{LUMO}	−0.254	−0.376	0.643*	0.687*	1.000			
CCR	0.859*	0.570	−0.996*	−0.999*	−0.692*	1.000		
$E_{LUMO} + E_{HOMO}$	−0.073	−0.293	0.489	0.541	0.960*	−0.546	1.000	
μ	−0.205	0.126	0.275	0.257	0.193	−0.255	0.117	1.000

* Correlation is significant at the 0.01 level.

TE and ΔH_f. The second PLS component is loaded primarily on two descriptors μ and E_{LUMO}. μ is expected to reflect the affinity for leaching to some extent. The descriptor E_{LUMO} accounts for the ability of the molecule to accept electrons from others in the process of photolysis. Thus, the lower the value of E_{LUMO}, the higher possibility the molecule accepts electrons. This study indicates that PAHs with lower E_{LUMO} value will be easier to be photodegraded and an increasing of μ and E_{LUMO} values could lead to the decreasing of disappearance rates for the second phase in chamber A. Fourth, the first PLS component is loaded primarily on descriptors M_w, TE, EE and CCR in model (3), which implies that these descriptors are highly inter-correlated. As indicated by the pseudo-regression coefficients for these descriptors, increasing M_w and CCR values or decreasing TE and EE values of the PAHs could lead to the decreasing photolysis rates of PAHs in chamber B. The descriptors M_w and CCR correlate with TE and EE negatively, as shown in Table 4. Thus, the increasing of M_w values of the PAHs leads to the increasing of $\log k_B$ values, which is consistent with that in models (1) and (2). The second PLS component is loaded primarily on the descriptor E_{LUMO}. It can be seen from model (3) that the increasing of E_{LUMO} values could lead to the decreasing of PAH disappearance rate in chamber B.

4. Conclusions

The photolysis of fly ash particle-associated PAHs deposited on glass slides follows first-order kinetics under simulated sunlight irradiation. Two phases of photolysis kinetics were observed for PAHs irradiated by simulate sunlight containing UV-B. The rate constants of PAHs in the first phase (0–50 h) range from $(2.5 \pm 0.1) \times 10^{-3}\ h^{-1}$ for benzo[*e*]pyrene to $(9.1 \pm 0.8) \times 10^{-3}\ h^{-1}$ for acenaphthylene, which are far greater than those observed in the second phase (50–550 h). The migration of PAHs from the interior to exterior of fly ash particles could be the rate-limiting step and thus prohibit the photolysis of the PAHs. Using simulated sunlight without UV-B, the PAH photolysis rate constants were significant lower, suggesting UV-B-radiation could accelerate photolysis of PAHs associated with fly ash particles. Moreover, three PLS analysis models were developed to explain the molecular structural characteristics governing the photolysis rates of PAHs in chambers A and B. The results suggested that the photolysis rate constants of PAHs decrease with the increasing of M_w, E_{LUMO}, $E_{LUMO} + E_{HOMO}$ and ΔH_f values.

Acknowledgements

The research was supported by the Scientific Research Foundation for the Returned Overseas Chinese Scholars, State Education Ministry and the National Basic Research Program of PR China (973 Project, 2002CB412409).

References

[1] F.E. Speizer, Environ. Health Perspect. 70 (1986) 9–15.
[2] J. Jocob, Pure Appl. Chem. 68 (1996) 301–308.
[3] S. Matsuzawa, L. Nasser-Ali, P. Garrigues, Environ. Sci. Technol. 35 (2001) 3139–3143.
[4] S. Fioressi, R. Arce, Environ. Sci. Technol. 39 (2005) 3646–3655.
[5] F. Reisen, J. Arey, Environ. Sci. Technol. 39 (2005) 64–73.
[6] R.G. Zepp, P.F. Schlotzhauer, in: P.R. Jones, P. Leber (Eds.), Polynuclear Aromatic Hydrocarbons, Ann Arbor Science Publishers, Ann Arbor, MI, 1979, pp. 141–158.
[7] T.D. Behymer, R.A. Hites, Environ. Sci. Technol. 19 (1985) 1004–1006.
[8] K.-M. Lehto, E. Vuorimaa, H. Lemmetyinen, J. Photochem. Photobiol. A: Chem. 136 (2000) 53–60.
[9] J.S. Miller, D. Olejnik, Water Res. 35 (2001) 233–243.
[10] H.A. Bamford, J.E. Baker, Atmos. Environ. 37 (2003) 2077–2091.
[11] T. Mill, W.R. Mabey, B.Y. Lan, A. Baraze, Chemosphere 10 (1981) 1281–1290.
[12] G.K.-C. Low, G.B. Batley, C.I. Brockbank, J. Chromatogr. 392 (1987) 199–210.
[13] W.A. Korfmacher, D.F.S. Natusch, D.R. Taylor, G. Mamantov, E.L. Wehry, Science 207 (1980) 763–765.
[14] W.A. Korfmacher, E.L. Wehry, G. Mamantov, D.F.S. Natusch, Environ. Sci. Technol. 14 (1980) 1094–1099.
[15] T.D. Behymer, R.A. Hites, Environ. Sci. Technol. 22 (1985) 1311–1319.
[16] R.A. Yokley, A.A. Garrison, E.L. Wehry, G. Mamantov, Environ. Sci. Technol. 20 (1986) 86–90.
[17] J.F. Niu, J.W. Chen, D. Martens, X. Quan, F.L. Yang, A. Kettrup, K.-W. Schramm, Environ. Pollut. 123 (2003) 39–45.
[18] J.F. Niu, J.W. Chen, D. Martens, B. Henkelmann, X. Quan, F.L. Yang, H.K. Seidlitz, K.-W. Schramm, Sci. Total Environ. 322 (2004) 231–241.
[19] J.W. Chen, P. Yang, S. Chen, X. Quan, X. Yuan, K.-W. Schramm, A. Kettrup, SAR QSAR Environ. Res. 14 (2003) 97–111.
[20] J.F. Niu, L.P. Huang, J.W. Chen, G. Yu, K.-W. Schramm, Chemosphere 58 (2005) 917–924.
[21] P.G. Pearson, Proc. Natl. Acad. Sci. 83 (1986) 8440–8441.
[22] J.C. Faucon, R. Bureau, J. Faisant, F. Briens, S. Rault, Chemosphere 38 (1999) 3261–3276.
[23] K.-S. Kim, K.-H. Hong, Y.-H. Ko, M.-G. Kim, J. Air Waste Manage. Assoc. 54 (2004) 555–562.
[24] S.V. Kakareka, T.I. Kukharchyk, V.S. Khomich, Environ. Pollut. 133 (2005) 383–387.
[25] A.I. Scott, Interpretation of the Ultraviolet Spectra of Natural Products, Pergamon, Oxford, 1964.
[26] J.C.W. Chien, J. Phys. Chem. 69 (1965) 4317–4325.